Applied Physics A (2019) 125:850
https://doi.org/10.1007/s00339-019-3138-z

Applied Physics A
Materials Science & Processing

Synthesis of gold nanoparticles by pulsed laser-assisted reduction of aqueous gold precursor

Fateme Sahebi[1] · Mehdi Ranjbar[1] · Mehdi Torabi Goodarzi[1]

Received: 4 June 2019 / Accepted: 5 November 2019

Abstract

In this paper, colloidal gold nanoparticles (GNPs) were synthesized by Nd:YAG ($\lambda = 1064$ nm) pulsed laser-assisted reduction (PLAR) of aqueous $[AuCl_4]^-$. In this process, during laser ablation of a Mo target in DI water, a $[AuCl_4]^-$ precursor solution was being added dropwise in situ. UV–Vis absorption spectra showed distinct plasmonic absorption bands at 209 and 530 nm corresponding to Mo nanoparticles (NPs) and GNPs, respectively. Furthermore, no significant conversion for $[AuCl_4]^-$ was found when it was added to aged Mo NPs or when it was irradiated in the lack of the Mo target. Using transmission electron microscope (TEM) images, it was found that precursor concentration and laser-ablation time can affect the population or size of GNPs. In PLAR with a small amount of KI solution in water, the GNPs size increases to ~ 50 nm via an iodine-induced particle fusion mechanism. The reduction mechanism was discussed based on metastable species intercation, producing the cavitation bubble during laser ablation.

1 Introduction

Notable attention has been paid to gold nanoparticles (GNPs) synthesis, science and applications over the past few years [1–7]. Many papers on the synthesis methods based on reducing the gold precursors such as $[AuCl_4]^-$, mostly attempt to control shape, size, size uniformity, purity, and stability of GNPs [8, 9]. In addition, special attention is paid to being single-step, environmental compatibility, and cost-effectiveness in the synthesis route. Reducing $[AuCl_4]^-$ by chemical agents has been vastly used as a common chemical approach with desirable control on nanoparticles formation [10–15]. However, the long-term toxicity of the used solvents in the chemical method is one of the unsolved environmental problems [8, 16–18].

Today, pulsed lasers are used to process materials and promote many chemical processes [8, 19–33]. Pulsed laser irradiation of a target immersed in a liquid generates cavitation bubble, shock waves, and secondary photons followed by NP growth, solution reduction, and the target-solution combination [18, 34–48]. Major advantages of laser-based methods are producing surfactant-free long-term stable colloidal solutions of NPs, functional NPs for in situ functionalization, and highly pure final products [49].

As a physicochemical synthesis technique, PLAR has been frequently studied by multiple groups to make variety of NPs such as Au, SiO_2, Pt/Co, Cu, Zn, Carbide, Fe/Au alloy components, etc. [50–61]. For example, John et al. have reported fabrication of silica-GNPs using a femtosecond laser irradiation of a silicon target in a $KAuCl_4$ solution. They attribute silica-GNPs formation to reduction of $[AuCl_4]^-$ via dense electron plasma formation prior to the silicon species ejection from the target [59]. Irradiation of $[AuCl_4]^-$ solution directly with a 532 nm nanosecond laser by Rodrigues et al. has produced uniform 5 nm GNPs via a plasmon-mediated photothermal catalytic growth [54]. Roske et al. have conducted laser irradiation of Cu and Zn targets in water or aqueous solutions of Cu and Zn [61]. In contrast to possible metal oxide formation in water, they have observed formation of more complex phase-pure nanomaterials such as $CuCl_2$, $Cu_2Cl(OH)_3$, $Zn_5(OH)_8Cl_2{\cdot}H_2O$, or layered zinc hydroxide nitrate, $Zn_5(OH)_8(NO_3)_2{\cdot}2H_2O$ in solutions. Hu et al. have developed tandem laser ablation synthesis in solution-galvanic replacement to make PtCo nanoalloys with different degree of alloying by controlling pH and the precursor concentration [60]. Furthermore, Dai et al. irradiated tungsten target installed in the $HAuCl_4$ solution with a 1064 nm pulsed laser and obtained Au-decorated

✉ Mehdi Ranjbar
ranjbar@cc.iut.ac.ir

[1] Department of Physics, Isfahan University of Technology, 84156-83111 Isfahan, Iran

Published online: 19 November 2019

WO_3 with enhanced ethanol sensing performance [62]. We also conducted PLAR using W, Au, and Ag target-ablation in $PdCl_2$ or $FeCl_3$ solution in which NPs of Pd/WO_3 [63], Pd/Ag and $AgCl_3$ [64], Pd/Au [65], and Fe/Au [66] have been obtained.

Although numerous studies have been done so far, further experiments, using a broader range of target/solution, could shed more light on PLAR technique. Recent works by others and us has established that a colloidal solution of MoO_{3-x} NPs could be able to reduce aqueous $HAuCl_4$ to GNPs without any reducing or stabilizer agent [17, 67]. To our best knowledge no paper on PLAR has been published yet with Mo/$[AuCl_4]^-$ system. Therefore, for further studies, it might be possible to apply PLAR of $[AuCl4]^-$ with a Mo target.

The primary aim of this paper is to investigate experimentally GNP formation by PLAR using a Mo target. We explore the relationship between synthesis conditions such as precursor concentration, ablation time, adding surfactant, and different targets. TEM, XRD and UV–Vis were the characterization methods. Our overall investigations are helpful to develop laser material processing concept for fast, single-step and green NP fabrication approaches.

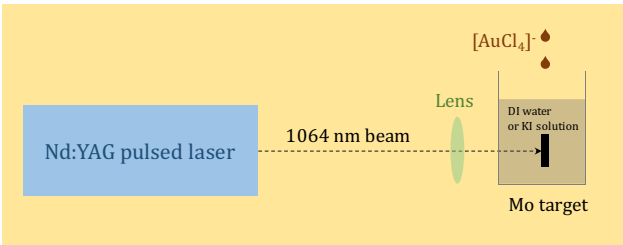

Fig. 1 Experimental setup scheme of the PLAR of gold precursor. GNPs are produced by in situ dropping of $[AuCl_4]^-$ into DI water during pulsed laser ablation of the Mo target. Other samples were prepared by adding KI into water

2 Materials and methods

2.1 Nanoparticle synthesis

Figure 1 shows a schematic representation for the PLAR experimental setup. NPs were prepared by PLAR of $[AuCl_4]^-$ solution using a Nd:YAG pulsed laser ($\lambda = 1064$ nm, pulse-width $\tau = 20$ ns, 600 mJ average pulse energy, and 10 Hz repetition rate). The laser beam was normally focused into a 2 mm^2 spot on a Mo target (99.99% purity) immersed into stirring 100 ml (80 mm liquid layer) of DI water. The gold precursor solution was prepared by dissolving $HAuCl_4$ powder (purchased from Sigma Aldrich and used as received) in DI water. 25 ml $HAuCl_4$ stock solution with 30, 50, 70, 90, 100, 200, 300, and 400 µM was added drop-by-drop during the laser exposure (in situ adding). In all of the processes, the total $HAuCl_4$ dropping time was set to the entire laser irradiation time. The final Au concentrations in all irradiated solutions were 6, 10, 14, 20, 18, 20, 40, 60, and 80 µM. Table.1 shows the sample name and their preparation conditions. For example, the sample denoted by S_{30}^{6} means ablation for 30 min with a 6 µM $[AuCl4]^-$ final concentration. During in situ dropping of the precursor, the base DI water gradually colored to violet, indicating formation of GNPs.

To investigate the effect of aging, 25 ml of 200 µM (final 40 µM) $HAuCl_4$ solution was added to 100 ml of a Mo colloidal solution 60 min after the end of ablation process (S_{aged}).

For investigating the effect of iodine on GNP growth, a base solution was made by adding 0.5 ml of 0.01 M KI solution to 100 ml DI water. For this case a 25 ml of 400 µM $HAuCl_4$ (final 80 µM irradiated solution) was used as dropping gold precursor (S_{KI} in Table.1).

Table 1 Sample names and preparation conditions

Sample name	Medium	$[AuCl_4]^-$ final concentration	Adding method	Ablation time (min)	Target
S_{30}^{0}	100 ml DI water	0	–	30	Mo
S_{aged}	100 ml DI water	40 µM	After aging	30	Mo
S_{30}^{80*}	100 ml DI water + 25 ml $HAuCl_4$	80 µM	–	30	–
S_{30}^{6-80}	100 ml DI water	6, 10, 14, 20, 18, 20, 40, 60 and 80 µM	In situ dropwise	30	Mo
S_{30-90}^{80}	100 ml DI water	80 µM	In situ dropwise	30, 45, 60, 75 and 90	Mo
S_{KI}	100 ml DI water + KI	80 µM	In situ dropwise	30	Mo

2.2 Characterizations

For obtained nanoparticle solutions, optical absorption spectra were measured in a 1-cm wide quartz cuvette using a Perkin-Elmer (Lambda25) UV–Vis spectrophotometer in the 190–1100 nm wavelength range. The TEM and SAED analyses were performed by Philips CM30 TEM apparatus. XRD pattern was acquired by Phillips XPERT X-ray diffraction apparatus at 2θ range of 10–80°.

3 Results and discussions

3.1 The effect of precursor adding method

We attempt to explore the nature of colloidal nanoparticles obtained by laser ablation of Mo in DI water by UV–Vis spectrophotometry. Figure 2a indicates the absorption spectra for sample S_{30}^{0}(see Table 1) at different aging period. For all the aging time, there is no observable absorption in the 300–800 nm region and the solution is highly transparent. However, a sharp absorption peak exists at 209 nm attributed to plasmonic or inter-band transition absorption of metallic Mo [68]. On the other hand, if defective Mo oxide (MoO_{3-x}) presents it would exhibit a broad band absorption peak in 400–1100 nm region due to the collective oscillation of electrons (the plasmonic effect) trapped in O vacancies [69–73].

A typical TEM image with its corresponding SAED pattern (inside part (b)) taken from the sample S_{30}^{0} reveals 50 nm crystalline NPs. The SAED analysis reveals formation of crystalline Mo and MoO_3 compounds during the laser ablation process. Any attempt to detect the presence of Mo or Mo oxide in the XRD pattern (Fig. 2c) failed because the amount of material available is probably below the sensitivity limit of used XRD machine. Nonetheless, adding H_2O_2 as a strong oxidation agent, red-shifts the spectrum considerably and causes the appearance of a sharp absorption edge at about 430 nm. The absorption edge is equivalent to a 3.2 eV band gap, indicating that a MoO_3 composition is formed only if an oxidant is added [74]. However, the observed

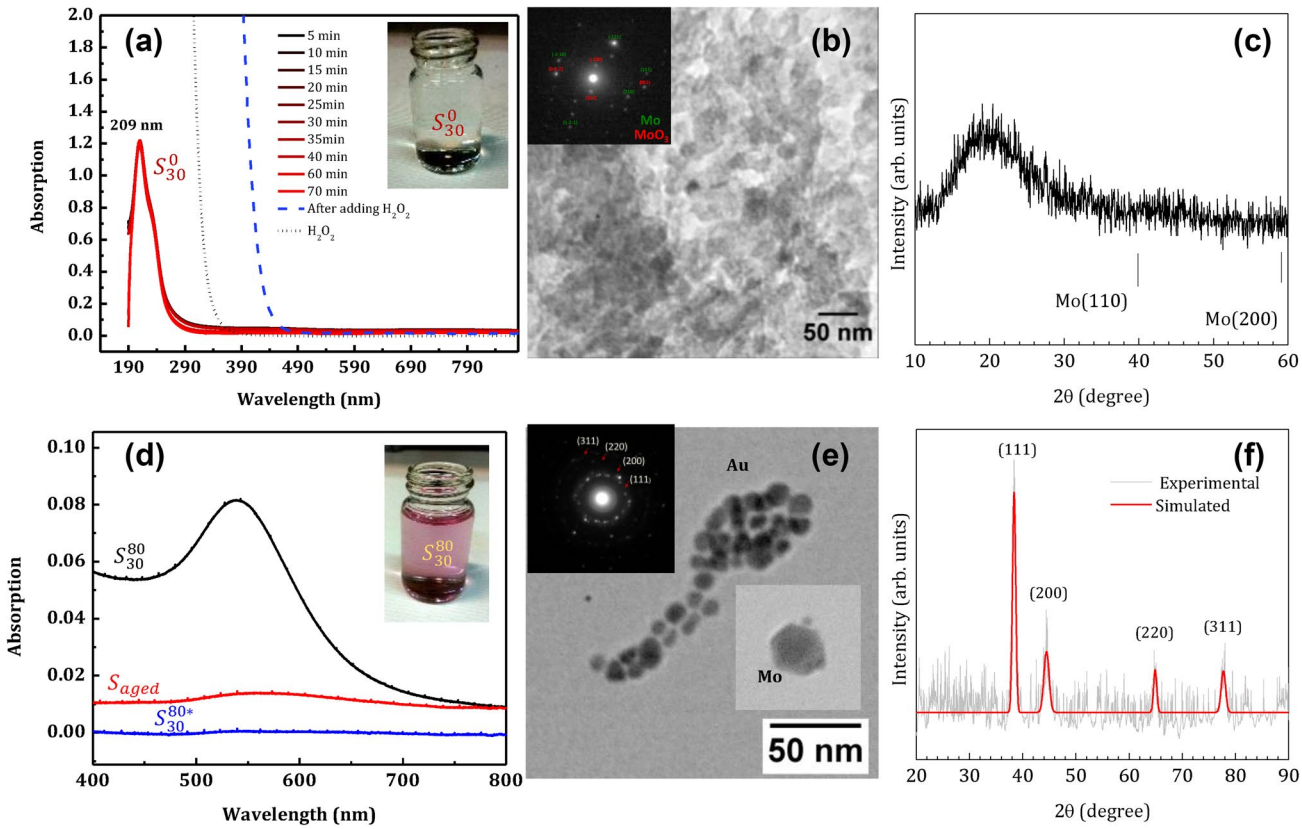

Fig. 2 **a** A photographic image and optical absorption spectra of S_{30}^{0} at different aging times from 5 to 70 min. The peak at 209 nm is attributed to plasmonic absorption of metallic Mo NPs. After addition to low concentration H_2O_2 a shoulder at near 480 nm appears. The optical absorption spectrum of H_2O_2 is also shown for comparison. **b** A typical TEM image along with a SAED pattern and **c** XRD pattern of nanoparticles in sample S_{Mo}. **d** Comparison of optical absorption spectra of S_{aged}, S_{30}^{80*} and S_{30}^{80}. Inside shows a photographic image of sample S_{30}^{80}. **e** TEM image and SAED pattern of GNPs in S_{30}^{80}. The Inset shows a particle attributed to molybdenum. **f** A typical XRD pattern of GNPs in sample S_{30}^{80}

sharp absorption edge could be intrinsically attributed to hydrogen peroxide absorption spectrum. To understand this, the pure spectrum of H_2O_2 used in our study is also shown in Fig. 2a. As can be seen, the spectrum of H_2O_2 has and absorption edge at 340 nm, which does not overlap the other spectra.

When $[AuCl_4]^-$ is added to sample S_{30}^0 after finishing laser ablation (= S_{aged}), no remarkable absorption peak appears (Fig. 2d). However, as Fig. 2d shows for sample S_{30}^{80}, when $[AuCl_4]^-$ is being dropped into the DI water during laser ablation of Mo (in situ method), the ablation environment turned purple and an absorption peak at 530 nm (Fig. 2d) appears indicating successfully formation of GNPs. This observation suggests that the in situ route likely allows the dropping gold precursor to interact with the plasma plume. Generally, in many chemical reactions the solvents should be added slowly drop-by-drop to prevent undesirable effects such as precipitation, thermalization, etc. In our case, to prevent any possible reaction between the precursor and the Mo target, we slowly dropped the gold salt solution in other part of experiments. In addition, the pre-added salt solution may reduce the laser power on the target surface.

It is demonstrated that, direct laser-$[AuCl_4]^-$ solution interaction has led to GNP formation [54]. However, as Fig. 2d (sample S_{30}^{80*}) shows, no Au LSPR absorption peak appears when $[AuCl_4]^-$ solution exposed to our 1064 nm laser beam in the lack of Mo target. Rodrigues et al. have reported that no $[AuCl_4]^-$ conversion occurs when being irradiated with 1064 nm pulses, while a 532 nm wavelength is able to do the conversion process [54]. They attributed the particle growth to an autocatalytic reduction kinetic via thermal dissociation of $[AuCl_4]^-$ by two or three photon-excitation at 532 nm and subsequently photothermal heating via surface plasmon absorption by newly formed GNPs. Therefore, it is likely that the presence of a target has distinctive role in the in situ reduction rout by 1064 nm wavelength.

TEM image of sample S_{30}^{80}, Fig. 2e, shows a chain of spherical NPs with 10 nm mean size [75], and the SAED pattern reveals the FCC structure of metallic gold. Inside the figure shows a ~ 35 nm hexagonal Mo particle with small spherical particle attached to its surface. Zamora et al. have attributed such configuration to a MoO_x/Mo combined with a tiny oxide layer [68]. In part (f), the XRD pattern of sample S_{30}^{80} represents (111) (200) (220) and (311) peaks, in agreement with the SAED pattern, related to the FCC cubic crystal structure of gold (JCPDS card number 00-001-1174).

3.2 The effect of the precursor concentration and ablation time

Following investigates the effect of $[AuCl_4]^-$ concentration and ablation time on the GNPs' morphology and plasmonic properties. Figure 3a shows the GNPs absorption spectra and absorption maximums for samples S_{30}^{6-80}. From the data, it can be seen that the Au plasmonic peak intensifies almost linearly in the 6–40 μM range, meeting the Beer–Lambert's law [76]. Then it does not change considerably at higher concentrations which likely needs longer ablation time. Comparing TEM images of S_{30}^{6} (Fig. 3b) with S_{30}^{80} (Fig. 2e) reveals that when concentration increases from 6 to 80 μM, the size of particles increase from 4 to 10 nm. TEM image of S_{30}^{6} also exhibits a more uniform size distribution compared to S_{30}^{80}.

Above results, indicate that the conversion process can be limited by the ablation time. To account for the effect of the ablation time, the PLAR process was performed with 30, 45, 60, 75, and 90 min ablation at a constant concentration (samples S_{30-90}^{80}). Figure 3c illustrates the corresponding absorption spectra and the maximum absorptions vs. time. Clearly, the absorption increases with ablation time up to 75 min and then remains almost constant. Furthermore, comparison of Fig. 3a, c implies that samples S_{30}^{40} and S_{60}^{80} show optimal states in which the minimum time for complete conversion is satisfied. This also suggests that doubling of concentration from 40 to 80 μM, doubles the required time for laser processing (from 30 to 60 min).

Figure 3d shows the TEM image and a size distribution histogram for S_{75}^{80}. Comparing it with TEM image of S_{30}^{80} (Fig. 2e) indicates that for a constant concentration, as the time increases from 30 min (Fig. 2e) to 75 min, the average particle size remains almost 10 nm, but the particles population clearly increases with irradiation time.

3.3 The effect of adding KI

Aggregation of noble metal nanoparticles is usually undesirable and should be avoided. Literature shows that the adsorbed iodine on GNPs, persuade them to aggregate or fuse through a surface charge neutralization process [77, 78]. Therefore, it is expected that adding an iodine like KI solution to the ablation medium affects the size or agglomeration of GNPs. Figure 4c compares the Au plasmonic absorption peaks in the absence (S_{30}^{80}) and presence of KI (S_{KI}).

From the presented data in the figure, it is apparent that small amount of KI solution dramatically enhances the plasmonic absorption. The KI solution was intrinsically transparent and, of course, for providing more evidence their optical absorption spectra were also recorded separately. As can be seen, there are no specific absorption peaks for KI solution. Furthermore, TEM images of the sample prepared with KI (Fig. 4d) represent individual GNPs of 50–60 nm mean size, about 10 times bigger than that of with pure DI water (Fig. 2e). Having different contrasts, binary NPs were detectable in various TEM images of the sample made with KI (Fig. 4d, right panel) probably originating from a Mo to Au nanoparticle fusion. One can

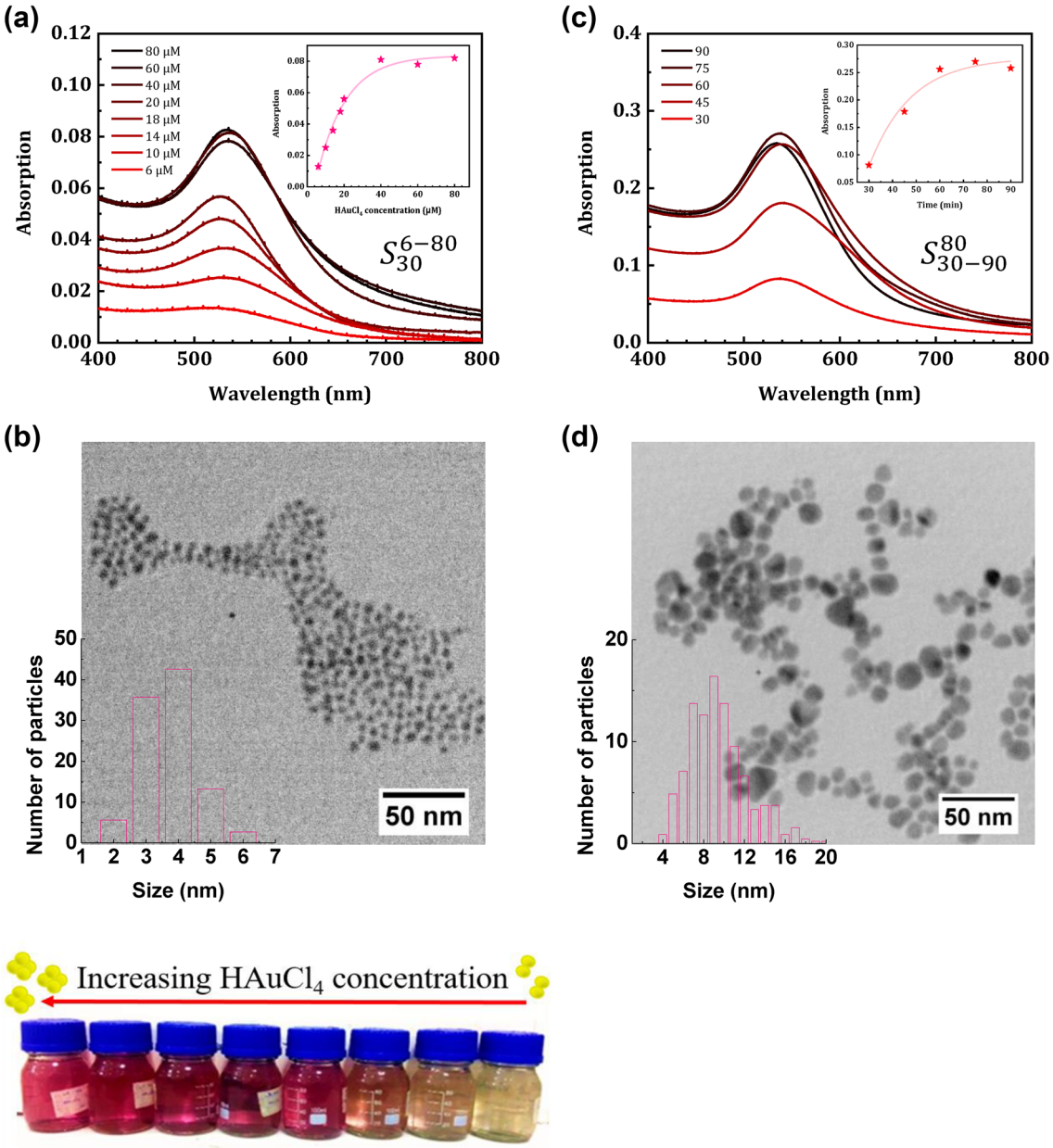

Fig. 3 Optical absorption spectra and peak intensity vs. concentration for samples S_{30}^{6-80} (**a**), and a typical TEM image taken from S_{30}^{6}. lower panel indicates the photographic images for samples S_{30}^{6-80}. **c** Optical absorption spectra for samples S_{30-90}^{80}. **d** TEM image corresponding to S_{75}^{80}. Lower panel: a photographical image of different sample with increasing $[AuCl_4]^-$ concentration. (The true color deepness of the samples increases with increasing the gold salt concentration, however, the visual difference has been due to the lack of proper lighting during taking photo)

express that the chemisorbed iodine atoms on newly formed GNPs increase the van der Waals attraction forces between the iodine-coated NPs acting as a "glue" leading to particle fusion to make bigger gold or even binary NPs. Moreover, during irradiation the Mo target, destabilized Au-iodine particles could grow to larger sizes or attached to other type of nanoparticles as TEM shows (see dashed circle). Re-irradiation may also occur for molybdenum species ejected into the ablation liquid, exited them to higher chemical activity states (Eq. 1), and enable them to reduce gold cations [79].

In laser-assisted reduction process, the mechanism for gold nanoparticles formation can be attributed to surface reduction reactions in the presence of particles or clusters. In this mechanism, after the interaction of laser beam with target, a cavity bubble is formed, in which the metastable species of the target material (Mo^*) and environment (H_2O^*,

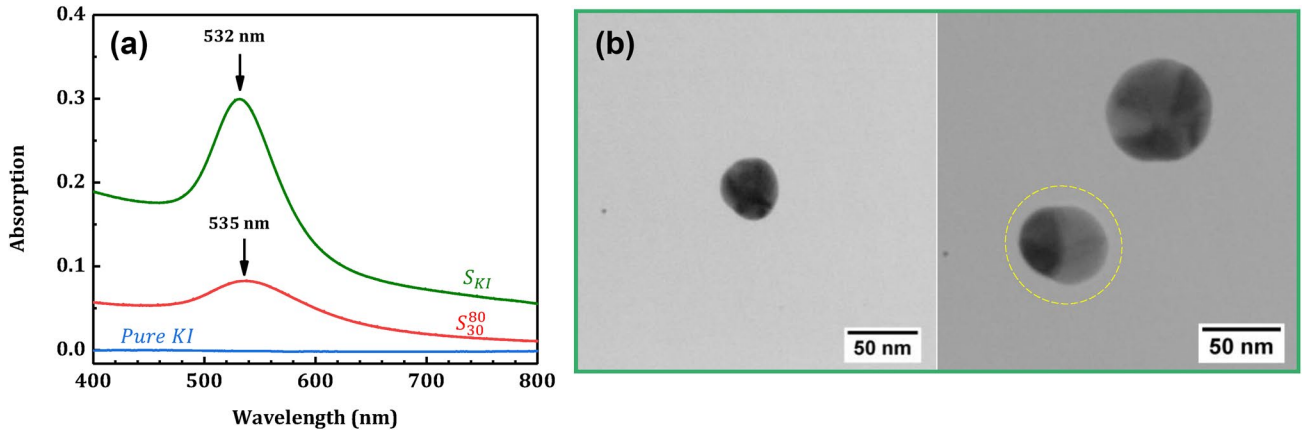

Fig. 4 **a** Comparison of optical absorption spectra of S_{30}^{80} and S_{KI}. The spectrum of KI solution is also shown for comparison for which no intrinsic absorption bands exist. **b** TEM images of NPs in S_{KI} taken from different points. Dashed circle indicates formation of binary NPs

$[AuCl_4]^{-*}$) are created. Generally, pressure and species density in this cavity bubble become high so that the thermodynamic conditions reach a non-equilibrium state [16]. These non-equilibrium thermodynamic conditions lead to ultra-complex chemical reactions that are not possible in the normal thermodynamic condition [18]. The proposed formation pathway of metastable species of Mo can briefly formulated as follows [80]:

$$\begin{aligned}
&Mo_{bulk} + h\nu \rightarrow Mo_{plasma}\\
&Mo_{plasma} \rightarrow Mo_{cluster}\\
&xMo_{cluster} + (m+n)H_2O \rightarrow Mo_xO_m \cdot nH_2O + mH_2O \uparrow \qquad (1)\\
&Mo_xO_m \cdot nH_2O \rightarrow 2nH^+ + \left[Mo_xO_{m+n}\right]^{2n-}\\
&y\left[Mo_xO_{n+m}\right]^{2n-} \rightarrow \left[Mo_{xy}O_{(m+n)y}\right]^{(2ny)-}.
\end{aligned}$$

The freshly prepared metastable molybdenum oxide isopoly anions are extremely reactive and ready to play the reducing role versus metal anions.$[AuCl_4]^-$ in the environment, can be reacted and reduced by the metastable species created by the cavity bubble:

$$\begin{aligned}
&H^+\left[AuCl_4\right]^- + \left[Mo_{xy}O_{(m+n)y}\right]^{(2ny)-}\\
&\quad \rightarrow Au^0 + 4Cl^- + 2H^+ + \text{oxidation products.} \qquad (2)
\end{aligned}$$

Due to acidity of the prepared solutions, there may be the possibility of instantaneous formation of molybdate solutions, $Mo_7O_{24}{}^{6-}$ $Mo_7O_{24}^{6-}$ and $Mo_8O_{26}{}^{6-}$$Mo_8O_{26}^{4-}$, which are the predominant complex species in pH 3–5 [81]. Even though there is no evidence in our data, these isopolyanions are not reducible and observable in crystal structure and morphological analysis [81]. This suggests the possible reason for not observing the crystalline structures of molybdenum oxide by XRD (Fig. 5).

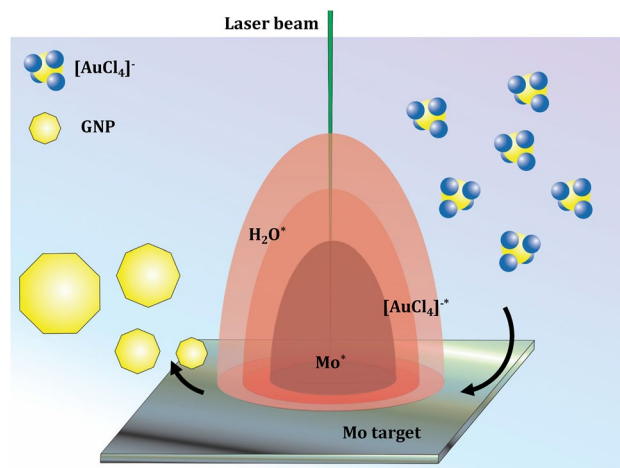

Fig. 5 A schematic representation of mechanism for laser-assisted reduction of $[AuCl_4]^-$

4 Conclusion

In summary, GNPs of < 10 nm dimension have been produced via a green method based on PLAR of $HAuCl_4$ solution. In this method, the precursor solution was added drop-by-drop simultaneously with the laser ablation of Mo target in DI water, which provides a desirable size distribution histogram. Moreover, it was found that the shape, dimension, and size distribution of the obtained GNPs can be manipulated by precursor concentration, ablation time and adding chemical such as KI.

Acknowledgements Authors would like to thanks Mr. A. R. Shafiyan for his kindly help in laser ablation experiments.

References

1. J.P. Sylvestre, A.V. Kabashin, E. Sacher, M. Meunier, Appl. Phys. A Mater. Sci. Process. **80**, 753 (2005)
2. X. Lu, M. Rycenga, S.E. Skrabalak, B. Wiley, Y. Xia, Annu. Rev. Phys. Chem. **60**, 167 (2009)
3. G.V. Hartland, Chem. Rev. **111**, 3858 (2011)
4. A. R. Sadrolhosseini, S. Abdul Rashid, S. Shafie, H. Soleimani, Appl. Phys. A Mater. Sci. Process. **125**, 0 (2019).
5. X. Wu, X. Tian, T. Chen, A. Zeng, G. Yang, Nanotechnology **29**, (2018).
6. L. Wang, W. Ma, L. Xu, W. Chen, Y. Zhu, C. Xu, N. A. Kotov, in *Mater. Sci. Eng. R Reports* (2010), pp. 265–274.
7. M.A. El-Sayed, Acc. Chem. Res. **34**, 257 (2001)
8. H. Rabitz, Science (80–). **299**, 525 (2003).
9. X. Sun, X. Jiang, S. Dong, E. Wang, Macromol. Rapid Commun. **24**, 1024 (2003)
10. N. Pazos-Perez, F.J. Garcia De Abajo, A. Fery, R.A. Alvarez-Puebla, Langmuir **28**, 8909 (2012)
11. I. Ojea-Jiménez, F.M. Romero, N.G. Bastús, V. Puntes, J. Phys. Chem. C **114**, 1800 (2010)
12. J. Kimling, M. Maier, B. Okenve, V. Kotaidis, H. Ballot, A. Plech, J. Phys. Chem. B **110**, 15700 (2006)
13. R. Jin, Y. Cao, C. A. Mirkin, K. L. Kelly, G. C. Schatz, J. G. Zheng, Science (80–) **294**, 1901 (2001).
14. P. Raveendran, J. Fu, S.L. Wallen, Green Chem. **8**, 34 (2006)
15. J.K. Edwards, G.J. Hutchings, Angew. Chem. Int. Ed. **47**, 9192 (2008)
16. V. Amendola, M. Meneghetti, Phys. Chem. Chem. Phys. **15**, 3027 (2013)
17. M.A. Hosseini, M. Ranjbar, Plasmonics **13**, 1897 (2018)
18. V. Amendola, M. Meneghetti, Phys. Chem. Chem. Phys. **11**, 3805 (2009)
19. R. Bini, Acc. Chem. Res. **37**, 95 (2004)
20. D. Zhang, B. Gökce, Appl. Surf. Sci. **392**, 991 (2017)
21. J. Xiao, P. Liu, C.X. Wang, G.W. Yang, Prog. Mater. Sci. **87**, 140 (2017)
22. V. Amendola, S. Barcikowski, J. Colloid Interface Sci. **489**, 1 (2017)
23. D. Zhang, J. Liu, P. Li, Z. Tian, C. Liang, ChemNanoMat **3**, 512 (2017)
24. D. Zhang, B. Gökce, S. Barcikowski, Chem. Rev. **117**, 3990 (2017)
25. D. S. Zhang, J. Liu, C. H. Liang, Sci. China Physics, Mech. Astron. **60**, 74201 (2017).
26. V.S. Burakov, N.V. Tarasenko, N.A. Savastenko, Spectrochim Acta Part B At. Spectrosc. **56**, 961 (2001)
27. K.C. Harper, E.G. Moschetta, S.V. Bordawekar, S.J. Wittenberger, A.C.S. Cent, Sci. **5**, 109 (2019)
28. M.E. Corrales, J. González-Vázquez, G. Balerdi, I.R. Solá, R. De Nalda, L. Bañares, Nat. Chem. **6**, 785 (2014)
29. T. Stensitzki, Y. Yang, V. Kozich, A.A. Ahmed, F. Kössl, O. Kühn, K. Heyne, Nat. Chem. **10**, 126 (2018)
30. A.N. Hellman, K.R. Rau, H.H. Yoon, S. Bae, J.F. Palmer, K.S. Phillips, N.L. Allbritton, V. Venugopalan, Anal. Chem. **79**, 4484 (2007)
31. D. Kray, A. Fell, S. Hopman, K. Mayer, G.P. Willeke, S.W. Glunz, Appl. Phys. A Mater. Sci. Process. **93**, 99 (2008)
32. M. Dong, X. Mao, J.J. Gonzalez, J. Lu, R.E. Russo, Anal. Chem. **85**, 2899 (2013)
33. J.L. Gottfried, Appl. Opt. **51**, B13 (2012)
34. S. F. Silva, L. Coelho, O. Frazão, J. L. Santos, F. X. Malcata, IEEE Sens. J. **12**, 93 (2012).
35. D. Amans, C. Malaterre, M. Diouf, C. Mancini, F. Chaput, G. Ledoux, G. Breton, Y. Guillin, C. Dujardin, K. Masenelli-Varlot, P. Perriat, J. Phys. Chem. C **115**, 5131 (2011)
36. M.A. Gondal, T.A. Saleh, Q.A. Drmosh, Appl. Surf. Sci. **258**, 6982 (2012)
37. N. Bärsch, J. Jakobi, S. Weiler, S. Barcikowski, Nanotechnology **20**, (2009).
38. F. Taccogna, M. Dell'Aglio, M. Rutigliano, G. Valenza, A. De Giacomo, Plasma Sources Sci. Technol. **26**, (2017).
39. S. Li, Y. Zhao, Y. Jiang, Y. Zhang, J. Laser Appl. **26**, 022001 (2014)
40. Y. Li, O.R. Musaev, J.M. Wrobel, M.B. Kruger, J. Laser Appl. **28**, 022004 (2016)
41. J. Liu, L. Huang, X. Tian, X. Chen, Y. Shao, F. Xie, D. Chen, L. Li, Int. J. Nanomed. **12**, 1 (2017)
42. S. Wu, P. Wang, Y. Cai, D. Liang, Y. Ye, Z. Tian, J. Liu, C. Liang, RSC Adv. **5**, 9069 (2015)
43. J.P. Sylvestre, S. Poulin, A.V. Kabashin, E. Sacher, M. Meunier, J.H.T. Luong, J. Phys. Chem. B **108**, 16864 (2004)
44. K.K. Irikura, J.L. Beauchamp, J. Phys. Chem. **95**, 8344 (1991)
45. S. Wu, J. Liu, Z. Tian, Y. Cai, Y. Ye, Q. Yuan, C. Liang, A.C.S. Appl, Mater. Interfaces **7**, 22935 (2015)
46. Y. Wang, Y. Zhao, W. He, J. Yin, Y. Su, Thin Solid Films **544**, 88 (2013)
47. M. Dell'Aglio, R. Gaudiuso, O. De Pascale, A. De Giacomo, Appl. Surf. Sci. **348**, 4 (2015)
48. S. Reich, P. Schönfeld, P. Wagener, A. Letzel, S. Ibrahimkutty, B. Gökce, S. Barcikowski, A. Menzel, T. dos Santos Rolo, A. Plech, J. Colloid Interface Sci. **489**, 106 (2017).
49. N. G. Semaltianos, in *Handb. Nanoparticles* (2015), pp. 67–92.
50. T. Nakamura, Y. Herbani, D. Ursescu, R. Banici, R. V. Dabu, S. Sato, AIP Adv. **3**, (2013).
51. H. Belmouaddine, M. Shi, L. Sanche, D. Houde, Phys. Chem. Chem. Phys. **20**, 23403 (2018)
52. D. Zhang, C. Zhang, J. Liu, Q. Chen, X. Zhu, C. Liang, A.C.S. Appl, Nano Mater. **2**, 28 (2019)
53. A. Tymoczko, M. Kamp, C. Rehbock, L. Kienle, E. Cattaruzza, S. Barcikowski, V. Amendola, Nanoscale Horizons 1 (2019).
54. C.J. Rodrigues, J.A. Bobb, M.G. John, S.P. Fisenko, M.S. El-Shall, K.M. Tibbetts, Phys. Chem. Chem. Phys. **20**, 28465 (2018)
55. E. Jiménez, K. Abderrafi, R. Abargues, J.L. Valdés, J.P. Martínez-Pastor, Langmuir **26**, 7458 (2010)
56. P. Liu, H. Chen, H. Wang, J. Yan, Z. Lin, G. Yang, J. Phys. Chem. C **119**, 1234 (2015)
57. V. A. Ermakov, E. Jimenez-Villar, J. M. C. Da Silva Filho, E. Yassitepe, N. V. V. Mogili, F. Iikawa, G. F. De Sá, C. L. Cesar, F. C. Marques, Langmuir **33**, 2257 (2017).
58. I. N. Saraeva, N. Van Luong, S. I. Kudryashov, A. A. Rudenko, R. A. Khmelnitskiy, A. L. vovic. Shakhmin, A. Y. Kharin, A. A. Ionin, D. A. bertovich Zayarny, D. H. Tung, P. Van Duong, P. H. Minh, J. Photochem. Photobiol. A Chem. **360**, 125 (2018).
59. M.G. John, K.M. Tibbetts, Appl. Surf. Sci. **475**, 1048 (2019)
60. S. Hu, M. Tian, E.L. Ribeiro, G. Duscher, D. Mukherjee, J. Power Sources **306**, 413 (2016)
61. C.W. Roske, J.W. Lefler, A.M. Müller, J. Colloid Interface Sci. **489**, 68 (2017)
62. E. Dai, S. Wu, Y. Ye, Y. Cai, J. Liu, C. Liang, J. Colloid Interface Sci. **514**, 165 (2018)
63. M. Ranjbar, H. Kalhori, S. M. Mahdavi, A. I. Zad, J. Nanoparticle Res. **14**, (2012).
64. N. Mottaghi, M. Ranjbar, H. Farrokhpour, M. Khoshouei, A. Khoshouei, P. Kameli, H. Salamati, M. Tabrizchi, M. Jalilian-Nosrati, Appl. Surf. Sci. **292**, 892 (2014)

65. Z. Sheykhifard, M. Ranjbar, H. Farrokhpour, H. Salamati, J. Phys. Chem. C **119**, 9540 (2015)
66. M. I. Nouraddini, M. Ranjbar, P. J. Dobson, H. Farrokhpour, C. Johnston, K. Jurkschat, Appl. Phys. A Mater. Sci. Process. **123**, (2017).
67. Q. Yin, L. Tan, Q. Lang, X. Ke, L. Bai, K. Guo, R. Qiao, S. Bai, Appl. Catal. B Environ. **224**, 671 (2018)
68. N. Zamora-Romero, M.A. Camacho-Lopez, M. Camacho-Lopez, A.R. Vilchis-Nestor, V.H. Castrejon-Sanchez, S. Camacho-Lopez, G. Aguilar, J. Alloys Compd. **788**, 666 (2019)
69. X. Tan, L. Wang, C. Cheng, X. Yan, B. Shen, J. Zhang, Chem. Commun. **52**, 2893 (2016)
70. T. Bao, W. Yin, X. Zheng, X. Zhang, J. Yu, X. Dong, Y. Yong, F. Gao, L. Yan, Z. Gu, Y. Zhao, Biomaterials **76**, 11 (2016)
71. L. Jin, X. Zheng, W. Liu, L. Cao, Y. Cao, T. Yao, S. Wei, J. Mater. Chem. A **5**, 12022 (2017)
72. H. Yin, Y. Kuwahara, K. Mori, H. Cheng, M. Wen, H. Yamashita, J. Mater. Chem. A **5**, 8946 (2017)
73. S.H. Lee, H. Nishi, T. Tatsuma, Nanoscale **10**, 2841 (2018)
74. M. Ranjba, F. Delalat, H. Salamati, Appl. Surf. Sci. **396**, 1752 (2017)
75. Y. Liu, X.M. Lin, Y. Sun, T. Rajh, J. Am. Chem. Soc. **135**, 3764 (2013)
76. J. Clark, J. Chem. Educ. **39**, 1 (2016)
77. W. Cheng, S. Dong, E. Wang, Angew. Chem. Int. Ed. **42**, 449 (2003)
78. J.E. Millstone, W. Wei, M.R. Jones, H. Yoo, C.A. Mirkin, Nano Lett. **8**, 2526 (2008)
79. M. Fernández-Arias, M. Boutinguiza, J. del Val, E. Medina, D. Rodríguez, A. Riveiro, R. Comesaña, F. Lusquiños, F.J. Gil, J. Pou, Appl. Surf. Sci. **473**, 548 (2019)
80. H. Zhang, G. Duan, Y. Li, X. Xu, Z. Dai, W. Cai, Cryst. Growth Des. **12**, 2646 (2012)
81. M.T. Pope, Inorg. Chem. **11**, 1973 (1972)